Journal of Solid State Chemistry 183 (2010) 1521–1528

Contents lists available at ScienceDirect

Journal of Solid State Chemistry

journal homepage: www.elsevier.com/locate/jssc

First-principles study of the crystal and electronic structures of α-tetragonal boron

Wataru Hayami *, Shigeki Otani

Exploratory Nanomaterials Research Laboratory, National Institute for Materials Science, 1-1 Namiki, Tsukuba, Ibaraki 305-0044, Japan

ARTICLE INFO

Article history:
Received 22 January 2010
Received in revised form
19 April 2010
Accepted 25 April 2010
Available online 13 May 2010

Keywords:
α-Tetragonal boron
Crystal structure
Electronic structure
Density functional theory

ABSTRACT

The crystal and electronic structures of α-tetragonal (α-t) boron were investigated by first-principles calculation. Application of a simple model assuming 50 atoms in the unit cell indicated that α-t boron had a metallic density of state, thus contradicting the experimental fact that it is a p-type semiconductor. The presence of an additional two interstitial boron atoms at the 4*c* site made α-t boron semiconductive and the most stable. The cohesive energy per atom was as high as those of α- and β-rhombohedral boron, suggesting that α-t boron is produced more easily than was previously thought. The experimentally obtained α-t boron in nanobelt form had about two interstitial atoms at the 8*i* sites. We consider that the shallow potential at 8*i* sites generates low-energy phonon modes, which increase the entropy and consequently decrease the free energy at high temperatures. Calculation of the electronic band structure showed that the highest valence band had a larger dispersion from Γ to Z than from Γ to X; this indicated a strong anisotropy in hole conduction.

1. Introduction

Solid boron is known to have a variety of crystal structures. Two rhombohedral (α and β) and two tetragonal (α and β) structures have been known since the 1950s [1–4], and the γ-phase was recently discovered under high pressure [5]. There has been a lot of research into the properties of α- and β-rhombohedral (α-rh, β-rh) boron, revealing that these materials are p-type semiconductors under normal pressure [6,7]. In 2001, it was discovered that β-rh boron becomes superconductive under high pressure [8], and in 2007 α-rh was also reported to become superconductive under high pressure [9,10]. β-rh boron is experimentally easy to obtain from liquid phase, whereas α-rh boron can be produced by chemical vapor deposition (CVD) [6] using molten platinum as a flux [11], or by annealing the amorphous phase [12]. All of the crystal structures are constructed from icosahedral subunits, which consist of 12 boron atoms.

α-Tetragonal (α-t) boron has a controversial history. It was first synthesized in 1943 by Laubengayer et al. [13] using CVD, and its structure was analyzed in detail in 1958 by Hoard et al. [3]. The structure they determined is illustrated in Fig. 1. It has a space group $P4_2/nnm$; four B_{12} icosahedra and two interstitial atoms at 2*b* sites – (0, 0, 1/2) and (1/2, 1/2, 0) – make a total of 50 atoms in a unit cell. The experimental lattice constants were $a=8.743$ Å and $c=5.03$ Å. Hoard et al. suggested that several sites (2*a*, 4*c*, 4*d*, and 4*g*) would accept additional interstitial atoms. In 1971, however, Amberger et al. denied the existence of the α-t B_{50} phase and concluded that α-t boron cannot be synthesized without impurities such as carbon or nitrogen [14]. They proposed a model in which two B atoms at 2*b* sites are replaced by C or N atoms and about two B atoms are present at the interstitial sites, creating $B_{50}C_2$ or $B_{50}N_2$ [15,16]. In 1992, theoretical works by Lee et al. supported these results, showing that the total energies of $B_{50}C_2$ and $B_{50}N_2$ are lower than that of pure B_{50} [17]. Thereafter, there were few reported studies of α-t boron until 2000.

Synthesis of boron nanowires and other nanostructures has been reported since 2001 [18–25]. Some of these studies have insisted on obtaining α-t boron nanostructures [22–25]. It was inevitable in most of these cases that the nanostructured boron included impurities in the course of synthesis. In 2003, Wang et al. succeeded in synthesizing an α-t boron nanobelt by a laser ablation method, without the use of catalysts [23]. They detected no impurities in the α-t boron obtained; this was inconsistent with the view generally accepted since the experiment by Amberger et al. in 1971 [14–16]. We have theoretically proven that α-t boron has so small a surface energy that it could be more stable than the other polymorphs when a crystal is in nanoscale, and we have proposed a model in which the boron nanobelt is grown on the basis of a stable nucleus of α-t structure [26–28].

Kirihara et al. [29–31] measured the electronic conductivity of this α-t boron nanobelt and showed that it is a p-type semiconductor. They suggested that the conduction may be prompted by the hopping process, as seen in β-rh boron [7], or just by simple thermal activation. The existence of band gap was

* Corresponding author.
E-mail address: hayami.wataru@nims.go.jp (W. Hayami).

0022-4596/$ - see front matter © 2010 Elsevier Inc. All rights reserved.
doi:10.1016/j.jssc.2010.04.036

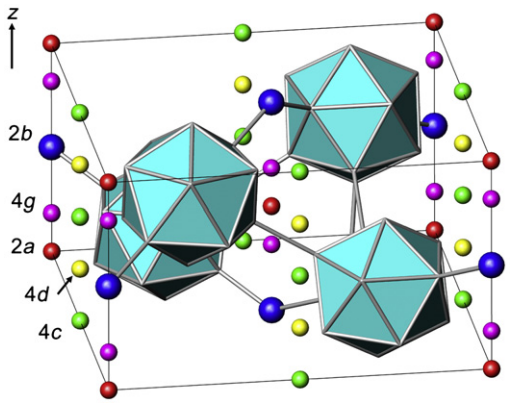

Fig. 1. Structure of α-tetragonal boron proposed by Hoard et al. Boron atoms at the apexes of the icosahedra and 2*b* sites (dark blue) make B_{50}. The interstitial sites are 2*a* (red), 4*c* (green), 4*d* (yellow), and 4*g* (pink). (For interpretation of the references to colour in this figure legend, the reader is referred to the web version of this article.)

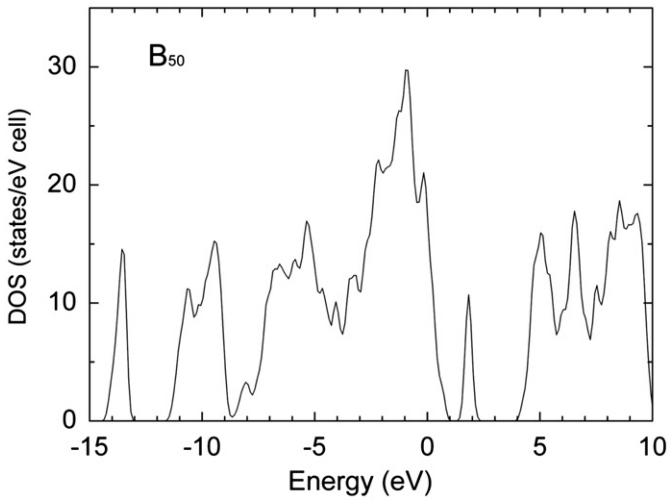

Fig. 2. Calculated DOS of B_{50} without interstitial atoms. The Fermi energy is set to zero.

also confirmed by electron energy loss spectroscopy (EELS) [32]. We calculated from first principles the density of states (DOS) of α-t boron, assuming that it has the structure of B_{50} proposed by Hoard et al. [3] as illustrated in Fig. 1. The results in Fig. 2 show that α-t boron is metallic, with holes at the top of the valence band; this is fundamentally consistent with the results of the previous work by Li et al. [33]. We considered that the additional interstitial atoms would decrease the holes in pure B_{50} and make it semiconductive. Hoard et al. roughly estimated the occupation ratio of the interstitial sites, but it differed depending on the sample [3]. It was 1/4 in 2*a* or 1/8 in 4*g* and 1/16 in 4*c* in one sample, and 1/16 in 4*g* and 1/8 in 4*c* in another sample. This implies that the presence of some interstitial atoms would help lower the total energy.

We investigated the amount and configuration of interstitial atoms that would stabilize α-t boron to the greatest extent and at the same time make it semiconductive. In the following sections, we examine how DOSs and cohesive energies depend on interstitial atoms, and we present the most probable structure for α-t boron. Finally, we compare our results with those of the latest structural analysis of the α-t boron nanobelt [34] and discuss the differences between them. The electronic band structures and electron densities are also provided.

2. Computational details

Calculation of electronic structures and geometry optimization were performed by using the CPMD code, version 3.13.2 [35–37]. This code is based on density functional theory with plane waves and pseudopotentials [38,39]. Norm-conserving Troullier–Martins-type pseudopotentials [40] in the Kleinman–Bylander form [41] were used. The generalized gradient approximation was included by means of the functional derived by Becke [42] and by Lee et al. [43]. An energy cutoff of 50 Ry was sufficient to provide a convergence for total energies and geometries. Geometry optimization and total energy calculations were done by using Monkhorst–Pack sampling [44] of a $(2\times2\times4)$ mesh. The test calculation was compared with that for a $(4\times4\times8)$ mesh. The difference in total energy per atom was about 4×10^{-4} eV. The calculations included no spins, because the unit cell has a large number of atoms (50–54). For DOS calculations, a $(6\times6\times12)$ mesh was used. Calculations were performed on a parallel computer using a message-passing interface.

3. Results and discussion

The interstitial sites suggested by Hoard et al. [3] for α-t boron are 2*a*, 2*b*, 4*c*, 4*d*, 4*e* and 4*g* (Fig. 1). Because the 4*e* sites – the centers of the icosahedra – are always empty and the 2*b* sites are

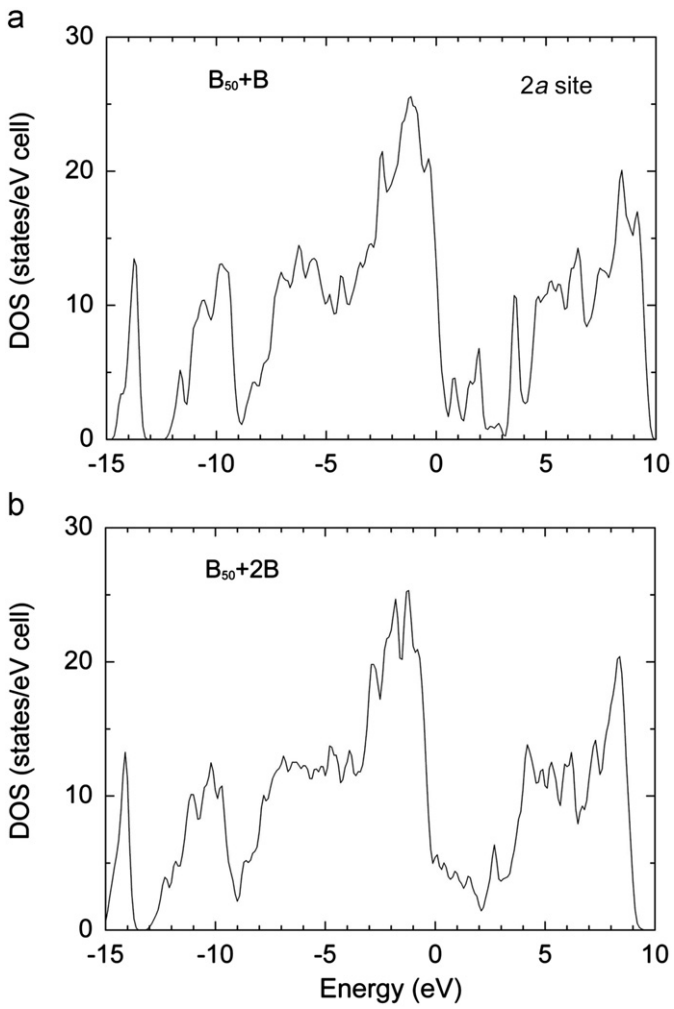

Fig. 3. Calculated DOSs of $B_{50}+nB$ ($n=1, 2$) at 2*a* sites. The Fermi energy is set to zero.

fully occupied [3], it was sufficient to investigate sites 2*a*, 4*c*, 4*d*, and 4*g*. We calculated the DOSs and cohesive energies with these sites partly occupied.

Fig. 3 shows the DOSs of systems that had one and two interstitial atoms at the 2*a* sites, i.e. (0, 0, 0) and (1/2, 1/2, 1/2). The Fermi energy was set to zero. The lattice constant *a* contracted from 8.85 to 8.74 Å and the constant *c* expanded from 4.98 to 5.06 Å as two atoms were inserted. With one atom inserted (a), although the Fermi level shifted toward the top of the valence band, the material remained metallic. When two atoms were inserted (b), the Fermi level shifted up to the top of the valence band, but then newly developed states filled the band gap keeping the material metallic. Thus, the presence of boron atoms at the 2*a* sites did not make the material semiconductive. The cohesive energies per atom were 5.883 eV (1 atom) and 5.844 eV (2 atoms); these were less (unstable) than that of B_{50} (5.913 eV; Table 1). Considering these facts, the 2*a* sites were unlikely to accept boron atoms.

With one atom placed at the 4*c* site, the cohesive energy per atom became 5.949 eV; this was higher than that of B_{50}, suggesting that the 4*c* site was favorable to interstitial atoms. Because the DOS was still metallic, with some holes in the valence band, we put two atoms at 4*c* sites. There were three configurations for having two atoms at four 4*c* sites: A, {(1/2, 0, 0), (0, 1/2, 0)}; B, {(1/2, 0, 0), (0, 1/2, 1/2)}; and C, {(1/2, 0, 0), (1/2, 0, 1/2)}. The optimized structures with configurations A and C had *a* axes of 8.83–8.86 Å and *c* axes of 5.04 Å. The *a* axes were almost the same as, and the *c* axes were longer than, that of the calculated B_{50} (a=8.85, c=4.98 Å). As for configuration B, the lattice lost fourfold symmetry and became orthorhombic (a=9.00, b=8.74, c=4.98 Å). The DOSs are shown in Fig. 4 (a)–(c), corresponding to the configurations A to C. The whole curves appear similar to each other, and all of the DOSs are semiconductive, with band gaps of 0.64, 0.07, and 0.32 eV, respectively. These small band gap values were close to the experimental value for the α-t nanobelt, as measured by Kirihara et al.; it was estimated to be 0.07 eV for the carrier activation energy.

The cohesive energies per atom were 5.972, 5.983, and 5.937 eV for configurations A, B, and C (Table 1). Configuration B had the greatest cohesive energy and the band gap closest to the experimental value. The values for A and B were larger than that of B_{50} and, surprisingly, close to the values for α-rh boron B_{12} and β-rh boron B_{105} (5.979 and 5.976 eV) calculated using the same method and under the same conditions. However, this does not mean that α-t boron is more stable than α- and β-rh boron, since the lattice shapes are different in each case, and besides, β-rh boron could be slightly more stable with defects and interstitial atoms [45–47]. In our previous work, we proved that nanosized α-t boron can be synthesized because of its low surface energy, even though it has a lower cohesive energy than α- and α-rh boron [26–28]. If α-t boron were to have a structure like that of configuration B, then α-t boron could be produced more easily than we expected. Because configuration C had a smaller cohesive energy than A, B, and the one-atom case, it was unlikely to occur. When three atoms were placed at 4*c* sites, the DOS became metallic (Fig. 4(d)). The cohesive energy per atom – 5.926 eV – was then lower than in the two-atom and the one-atom cases. It was therefore unlikely that 4*c* sites accepted three atoms.

The situation with 4*d* site occupation was similar to that in the 4*c* case. With one atom placed at the 4*d* site, the cohesive energy per atom became 5.939 eV, which was higher than that of B_{50} but not as high as in the 4*c* case. Because the DOS was metallic with one atom, we put two atoms at the 4*d* sites. As in the 4*c* case, there were three configurations for having two atoms in four 4*d* sites: A, {(1/2, 0, 1/4), (0, 1/2, 1/4)}; B, {(1/2, 0, 1/4), (0, 1/2, 3/4)}; and C, {(1/2, 0, 1/4), (1/2, 0, 3/4)}. The other configurations are symmetrically equivalent to one of these three. The optimized lattice constants (*a*, *c*) were (8.83, 5.00 Å) for configuration A and

Table 1
Cohesive energies per atom of B_{50}+*n*B, and band gaps.

Site	*n*	Configuration	Cohesive energy/atom (eV)	Band gap (eV)
–	0	(B_{50})	5.9130	
2*a*	1		5.883	0
2*a*	2		5.844	0
4*c*	1		5.949	0
4*c*	2	A (1/2, 0, 0), (0, 1/2, 0)	5.972	0.64
4*c*	2	B (1/2, 0, 0), (0, 1/2, 1/2)	5.983	0.07
4*c*	2	C (1/2, 0, 0), (1/2, 1/2, 0)	5.937	0.32
4*c*	3		5.926	0
4*d*	1		5.939	0
4*d*	2	A (1/2, 0, 1/4), (0, 1/2, 1/4)	5.956	0.87
4*d*	2	B (1/2, 0, 1/4), (0, 1/2, 3/4)	5.972	1.11
4*d*	2	C (1/2, 0, 1/4), (1/2, 0, 3/4)	5.899	0.70
4*d*	3		5.858	0
4*g*	1		5.888	0
4*g*	2	A (0, 0, *x*), (1/2, 1/2, 1/2+*x*)	5.867	0
4*g*	2	B (0, 0, *x*), (1/2, 1/2, 1/2−*x*)	5.863	0
4*g*	2	C (0, 0, *x*), (0, 0, −*x*)	5.889	0
4*g*	3		5.864	0
4*g*	4		5.868	0
2*a*, 4*c*	2	A (0, 0, 0), (0, 1/2, 0)	5.910	0.03
2*a*, 4*c*	2	B (1/2, 1/2, 1/2), (0, 1/2, 0)	5.914	0.18
2*a*, 4*d*	2	(0, 0, 0), (1/2, 0, 1/4)	unstable	
2*a*, 4*g*	2	(0, 0, 0), (1/2, 1/2, 0.688)	5.856	0
4*c*, 4d	2	(0, 1/2, 0), (1/2, 0, 1/4)	unstable	
4*c*, 4*g*	2	A (0, 1/2, 0), (1/2, 1/2, 0.688)	5.921	0
4*c*, 4*g*	2	B (0, 1/2, 0), (1/2, 1/2, 0.188)	5.914	0
4*d*, 4*g*	2	A (1/2, 0, 3/4), (1/2, 1/2, 0.188)	unstable	
4*d*, 4*g*	2	B (1/2, 0, 3/4), (0, 0, 0.188)	unstable	

n is the number of interstitial atoms.

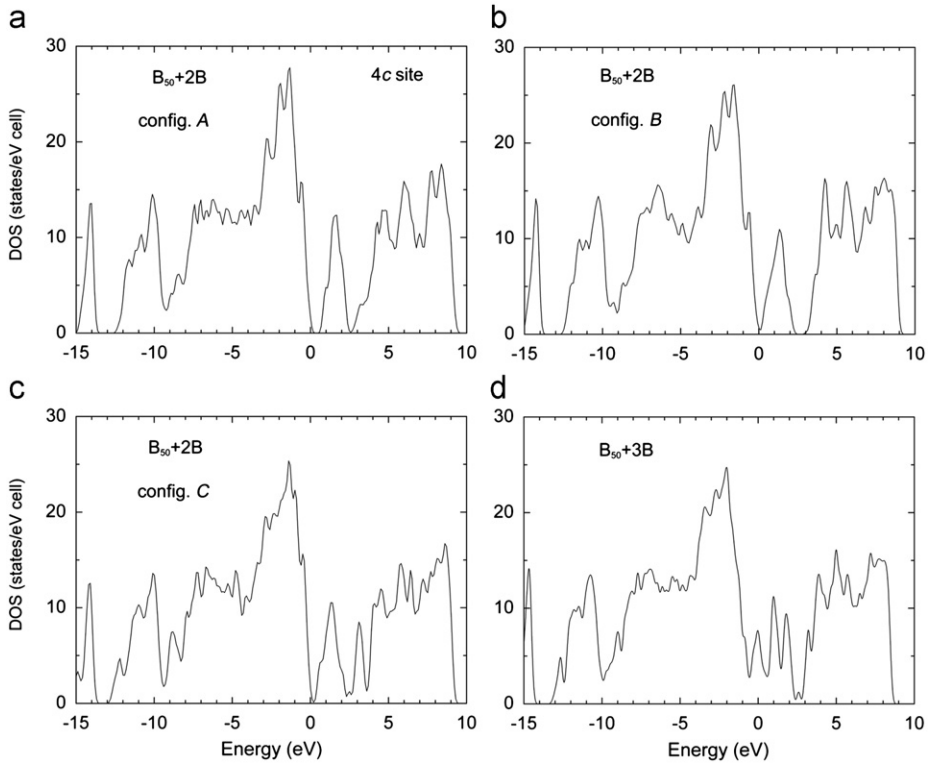

Fig. 4. Calculated DOSs of B_{50}+nB (n=2, 3) at 4c sites. The Fermi energy is set to zero.

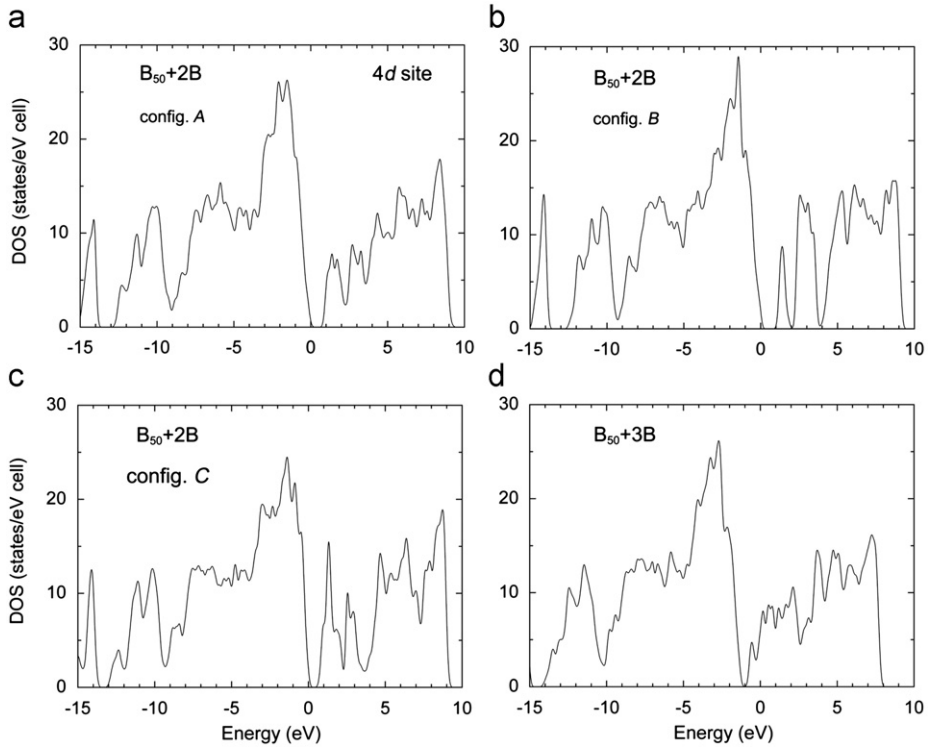

Fig. 5. Calculated DOSs of B_{50}+nB (n=2, 3) at 4d sites. The Fermi energy is set to zero.

(8.85, 5.00 Å) for configuration B. Configuration C was orthorhombic and (a, b, c) were (8.82, 8.83, 5.03 Å). The DOSs are shown in Fig. 5(a)–(c), corresponding to the configurations A to C. All the DOSs were semiconductive with band gaps of 0.87, 1.1, and 0.7 eV. These gaps were a little larger than those in the 4c cases (Fig. 4(a)–(c)) and deviated more from the experimental value (0.07 eV) [31]. The cohesive energies per atom were 5.956, 5.972, and 5.899 eV for configurations A, B, and C, respectively

(Table 1). Configuration B had the highest value, but it was not as high as that of configuration B in the case of 4*c*. When three atoms were put at 4*d* sites, the DOS became metallic (Fig. 5(d)). The cohesive energy per atom, 5.858 eV, was lower than that of B_{50}, so 4*d* sites would be unlikely to accept three atoms. These findings suggested that there were no reasons for 4*d* sites to be more favorable than 4*c* sites.

The 4*g* sites in Fig. 1 were mentioned by Hoard et al. as alternatives to the 2*a* site, because the vacancy at the 2*a* site is a little large for a boron atom. We first put an atom at (0, 0, 0.183) and optimized the structure. The atom then shifted to (0, 0, 0.189) and the cohesive energy per atom was 5.888 eV (higher than that of the 2*a* site but lower than that of B_{50}), suggesting that the 4*g* site was not very favorable for an interstitial atom. The DOS with one atom was metallic, with some holes (Fig. 6(a)). As in the cases of 4*c* and 4*d*, there were three configurations for putting two atoms at four 4*g* sites: A, {(0, 0, *x*), (1/2, 1/2, *x*)}; B, {(0, 0, *x*), (1/2, 1/2, $-x$)}; and C: {(0, 0, *x*), (0, 0, $-x$)}, where the optimized values of *x* were 0.200, 0.192, and 0.167, respectively. In contrast to the cases of 4*c* and 4*d*, all the DOSs with two atoms were not semiconductive but metallic. Fig. 6(b) shows the DOS of configuration A; those of configurations B and C were similar to this. The cohesive energies per atom of these configurations were 5.867, 5.863, and 5.889 eV, all of which were lower than that of B_{50}. When three and four atoms were put at 4*g* sites, the DOSs were still metallic (Fig. 6(c) and (d)). The cohesive energies per atom were 5.864 and 5.868 eV—again lower than that of B_{50}. Thus no number of interstitial atoms at the 4*g* sites would ever make B_{50} semiconductive or stable.

So far, we have studied cases in which sites 2*a*, 4*c*, 4*d*, and 4*g* are separately occupied. There are a number of combinations for the mixed occupation of these sites, and it is difficult to investigate all of them. Because two interstitial atoms made B_{50} semiconductive and the most stable in the cases of 4*c* and 4*d*, we assumed that two atoms were always necessary for mixed occupation. This reduced the number of combinations of sites to 6, some of which had several configurations. In total, there were 9 configurations, as listed in Table 1. Only (2*a*, 4*c*) A, B were stable and semiconductive; the other configurations were unstable {(2*a*, 4*d*), (4*c*, 4*d*), (4*d*, 4*g*) A, B}, or metallic {(2*a*, 4*g*), (4*c*, 4*g*) A, B}. In the unstable configurations, 4*d* atoms spontaneously shifted to the 4*c* sites. The only possible cases (2*a*, 4*c*) A, B had cohesive energies of 5.910 and 5.914 eV—much lower than those of the two-atom 4*c* and 4*d* cases. The mixed occupations therefore had no advantages over the separate occupations of sites 4*c* and 4*d*.

Considering the cohesive energies and band gaps examined so far (Table 1), we concluded that the most stable structure for α-t boron was B_{50} plus two interstitial B atoms at the 4*c* sites, i.e. (1/2, 0, 0) and (0, 1/2, 1/2) (configuration B). In the experiment by Hoard et al. [3], the occupation ratios of the interstitial sites were 1/4 at 2*a* or 1/8 at 4*g* and 1/16 at 4*c* in one sample, and 1/16 at 4*g* and 1/8 at 4*c* in another sample. In both cases, sites 2*a* or 4*g* were partly occupied, unlike in our result, and the total number of interstitial atoms was 3/4, which is less than our estimate of 2. However, it must be noted that the purity of the sample produced by Hoard et al. was questionable, because later experiments by Amberger et al. could not reproduce pure α-t boron by the same method [14–16].

It is highly probable that the α-t boron nanobelt produced by Wang et al. [23] is almost pure boron, because it was produced by a laser ablation method without catalysts and its lattice constants imply that it is purer than those produced in other studies [22,24,25]. We compared our results with the precise structural analysis of the nanobelt conducted recently by Hyodo et al. [34]. Their Rietveld analysis of the X-ray diffraction data showed that the occupation ratios of the interstitial sites were: 2*a*, 11%; 2*b*, 93%; 4*c*, 0%; 4*d*, 0%; 8*h*, 2%; and 8*i*, 24%. The total number of boron atoms was 52.2. Sites 8*h* and 8*i* here were not mentioned by Hoard et al. [3] but were proposed by Ploog et al. in relation to the structure of α-t $B_{50}C_2$ or $B_{50}N_2$ [15,16]. Their positions were: 8*h*: (0, 1/2, $\pm z$), (1/2, 0, $\pm z$), (0, 1/2, 1/2 $\pm z$), (1/2, 0, 1/2 $\pm z$), z=0.8557 and 8*i*: ($\pm x$, 0, 0), (0, $\pm x$, 0), (1/2 $\pm x$, 1/2, 1/2), (1/2, 1/2 $\pm x$, 1/2), x=0.433. Sites 8*h* and 8*i* can be regarded as 4*c* sites

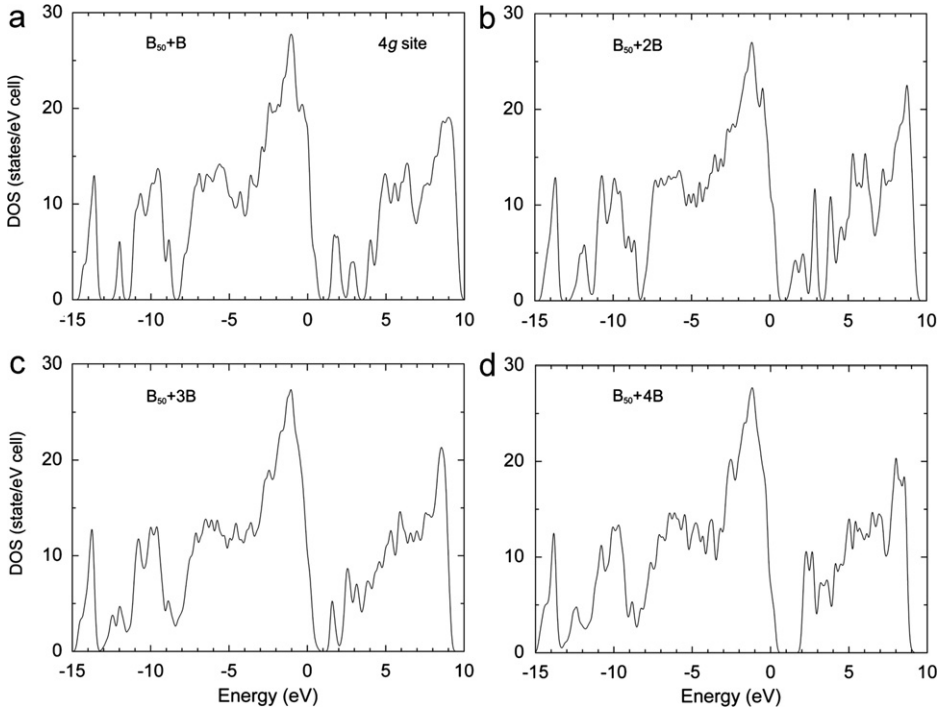

Fig. 6. Calculated DOSs of B_{50}+*n*B (n=1–4) at 4*g* sites. The Fermi energy is set to zero.

slightly deviated in the z direction ($8h$) and x, y direction ($8i$). Although the total number of atoms estimated by Hyodo et al. was close to ours, a large portion of the interstitial atoms was present at the $8i$ sites and, contrary to our results, no atoms were present at the $4c$ sites. To clarify the cause of the discrepancy, we investigated whether the $8i$ sites were favorable for interstitial atoms.

When one atom was placed at the $8i$ site, the atom shifted to the nearest $4c$ site, suggesting the $8i$ site to be neither stable nor metastable. There were four distinctive configurations for putting two atoms in $8i$ sites. In all these configurations, two atoms shifted to the $4c$ site, as in the one-atom case. However, when two atoms were placed at the $8i$ site (x, 0, 0) and the $4c$ site (0, 1/2, 0), the atom at the $8i$ site remained in a metastable state, as shown in Fig. 7. If the Rietveld analysis is correct, the $8i$ sites might be stabilized by a small number of defects at $2b$ and interstitial atoms at $2a$ in α-t nanobelts, although this could not be confirmed by the present calculations, which are based on B_{50} unit cells.

If this were the case, the preference of $8i$ sites may be explained as follows. Our calculations were conducted at zero temperature, whereas the boron nanobelt was synthesized at a high temperature by laser ablation followed by rapid quenching. Entropy must be taken into consideration at a finite temperature to calculate the free energy. Having atoms at $8i$ sites, α-t boron should have low-energy phonon modes owing to the shallow potential at the $8i$ sites (Fig. 7); these low-energy modes increase the entropy and consequently reduce the free energy at high temperature. As a result, under conditions of synthesis, B_{50}+2B at $8i$ sites should have a lower free energy than B_{50}+2B at $4c$ sites, because the difference in the total energy at zero temperature is very small. The experimental nanobelt probably maintains the $8i$-site structure after rapid quenching. This mechanism is similar to that proposed with respect to the phase transition from α-rh to β-rh boron where β-rh boron has softer phonon modes than α-rh boron [48].

The electronic band structure of B_{50}+2B at site $4c$ (configuration B) is shown in Fig. 8. The top of the valence band is almost at the Γ point (more precisely, at a k point between Γ and X) and the bottom of the conduction band is at the A point with an indirect band gap of 0.07 eV, very close to that of the experimental nanobelt, 0.07 eV [31]. Interestingly, the highest valence band had much greater dispersion from Γ to Z than from Γ to X, suggesting a strong anisotropy in hole conduction.

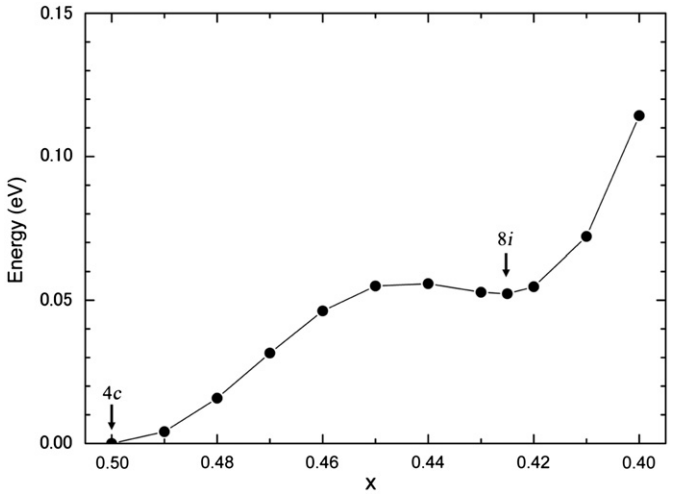

Fig. 7. Potential of a boron atom at the sites (x, 0, 0), x=0.5–0.4 with another atom placed at the $4c$ site (0, 1/2, 0).

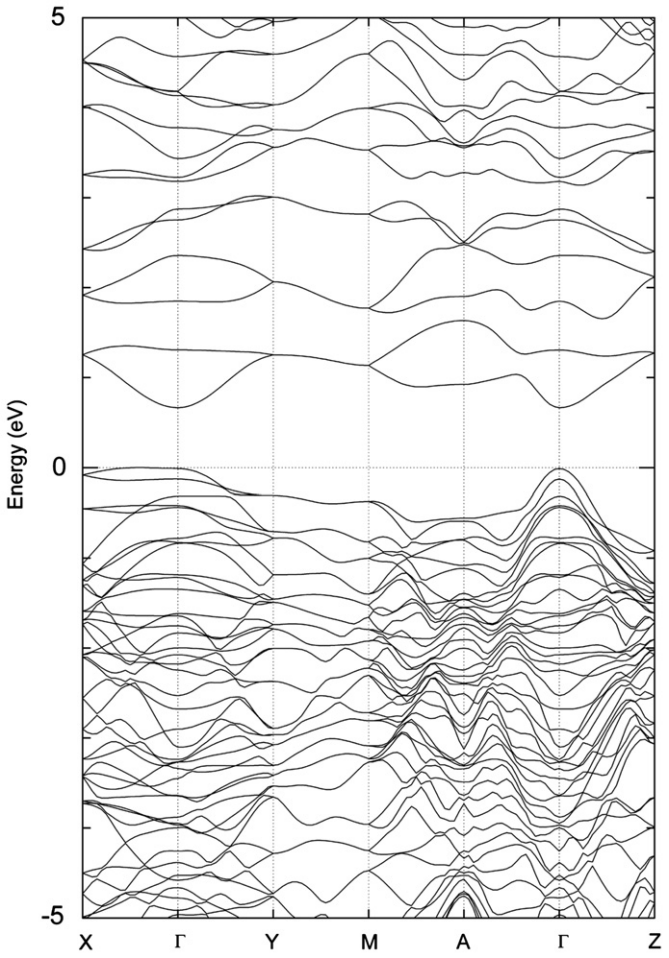

Fig. 8. Electronic band structures of B_{50}+2B at sites $4c$ (configuration B). The Fermi energy is set to zero.

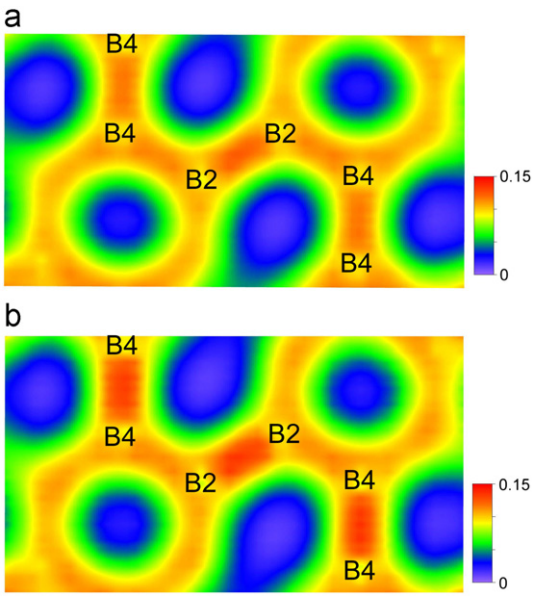

Fig. 9. Calculated electron densities of B_{50} (a) and B_{50}+2B at site $4c$ (b) (configuration B). Units are electrons/(a.u.)^3.

The electron densities of pure B_{50} and of B_{50}+2B at $4c$ (configuration B) are compared in Fig. 9. The indexes of the boron atoms, B2 and B4, follow the notation of Hoard et al. [3].

Table 2
Bond lengths of B_{50} and B_{50}+2B at sites 2*a*, 4*c*, 4*d*, and 4*g* in Å units.

Site (configuration)	Inter-bond to *z* (B4–B4)	Inter-bond to *x*, *y* (B2–B2)	B_{12}–2*b*	Intra-bond	B_{12}-site
B_{50} (calculated)	1.72	1.70	1.71	1.74–1.88	
2*a*	1.69	1.72	1.71	1.73–1.91	2.17
4*c* (B)	1.67	1.66	1.72	1.74–1.89	1.79
4*d* (B)	1.66	1.67	1.71	1.73–1.92	1.79
4*g* (C)	1.71	1.71	1.71	1.74–1.91	1.91

B_{12} is a boron icosahedron.

B2–B2 is an inter-icosahedral bond (inter-bond) along the *x* or *y* direction and B4–B4 is an inter-bond along the *z* direction. B2–B4 is an intra-icosahedral bond (intra-bond). In B_{50}, the density in the inter-bonds was only slightly higher than that in the intra-bonds. When two B atoms were inserted into the 4*c* sites, the density of the inter-bonds increased by about 20%. This feature by which the inter-bonds were stronger than the intra-bonds has also been observed in α-rh boron [49,50]. The change in electron density suggested that the interstitial B atoms stabilized B_{50} by strengthening the inter-icosahedral bonds. The bonds between the icosahedral B_{12} and 4*c* sites (not shown in the figure) were of the same density as the intra-bonds.

The calculated bond lengths (Table 2) supported the electron density results. The inter-bonds, which were 1.70–1.72 Å in B_{50}, contracted to 1.66–1.67 Å in the cases of 4*c* (configuration B) and 4*d* (configuration B), whereas those in 2*a* and 4*g* cases did less. The intra-bonds and the bonds between B_{12} and 2*b* sites changed little. Thus there is a correlation between the cohesive energy and the strength of the inter-icosahedral bonds.

4. Conclusions

Our first-principles calculations revealed that α-t boron B_{50} was most stable and semiconductive when it had two interstitial atoms at 4*c* sites (1/2, 0, 0) and (0, 1/2, 1/2) (configuration B). The total number of atoms, 52, was in good agreement with the experimental value of 52.2 [34]. The cohesive energy per atom, 5.983 eV, was much higher than that of B_{50} (5.913 eV) and was as high as those of α- and β-rh boron (5.979 and 5.976 eV, respectively) calculated by the same method and under the same conditions. Thus the synthesis of α-t boron may be easier than was previously considered [26–28]. However, this does not mean that α-t boron is more stable than α- and β-rh boron. The structure of α-t nanobelt has about two interstitial atoms at 8*i* sites [34]. According to our calculations, two atoms at 8*i* sites were unstable. However, an atom at the 8*i* site could be metastable when two atoms were placed at 8*i*(0.425, 0, 0) and 4*c*(0, 1/2, 0). A small number of defects at 2*b* and interstitial atoms at 2*a* might stabilize 8*i* sites in experimental nanobelts. The reason for the nanobelt preference of 8*i* sites over 4*c* sites is probably that a very shallow potential at the 8*i* site generates low-energy phonon modes that increases the entropy and, consequently, lower the free energy at a high temperature. Because the difference in cohesive energy between sites 4*c* and 8*i* was very small, it is probable that the 8*i*-site structure has a lower free energy at a high temperature. The nanobelt produced by laser ablation would maintain the 8*i*-site structure after rapid quenching.

Calculation of electronic band structures showed that the 4*c*-site structure had an indirect band gap of 0.07 eV which is very close to the experimental value [31]. The highest valence band had much greater dispersion from Γ to Z than from Γ to X, suggesting a strong anisotropy in hole conduction.

Mapping of the electron density and calculated bond lengths revealed that the presence of two B atoms at sites 4*c* strengthened the inter-icosahedral bonds by about 20%; the bond lengths accordingly contracted by about 3%. As has been observed in α-rh boron, we considered that the strong inter-icosahedral bonds contributed to the stability of α-t boron.

Acknowledgments

The authors thank Profs. K. Kimura, N. Koshizaki, K. Kirihara K. Soga, and H. Hyodo for their valuable discussions and for providing us with the experimental data before publication.

References

[1] B.F. Decker, J.S. Kasper, Acta Crystallogr. 12 (1959) 503.
[2] R.E. Hughes, C.H.L. Kennard, D.B. Sullenger, H.A. Weakliem, D.E. Sands, J.L. Hoard, J. Am. Chem. Soc. 85 (1963) 361.
[3] J.L. Hoard, R.E. Hughes, D.E. Sands, J. Am. Chem. Soc. 80 (1958) 4507.
[4] C.P. Talley, S. LaPlaca, B. Post, Acta Crystallogr. 13 (1960) 271.
[5] A.R. Oganov, J.H. Chen, C. Gatti, Y.Z. Ma, Y.M. Ma, C.W. Glass, Z.X. Liu, T. Yu, O.O. Kurakevych, V.L. Solozhenko, Nature 457 (2009) 863.
[6] F.H. Horn, J. Appl. Phys. 30 (1959) 1611.
[7] H. Werheit, H.G. Leis, Phys. Status Solidi 41 (1970) 247.
[8] M.I. Eremets, V.V. Struzhkin, H. Mao, R.J. Hemly, Science 293 (2001) 272.
[9] M. Kaneshige, K. Shimizu, H. Hyodo, K. Kimura, 48th High-Pressure Conf. Japan (2007) 1C06.
[10] K. Shirai, H. Dekura, A. Yanase, J. Phys. Soc. Jpn. 78 (2009) 084714.
[11] F.H. Horn, J. Electrochem. Soc. 106 (1959) 905.
[12] J.A. Ugai, N.E. Soloviev, in: A. Matkovich (Ed.), Boron and Refractory Borides, Springer, New York, 1977, p. 227.
[13] A.W. Laubengayer, D.T. Hurd, A.E. Newkirk, J.L. Hoard, J. Am. Chem. Soc. 65 (1943) 1924.
[14] E. Amberger, K. Ploog, J. Less Common Met. 23 (1971) 21.
[15] K. Ploog, H. Schmidt, E. Amberger, G. Will, K.H. Kossobutzki, J. Less Common Met. 29 (1972) 161.
[16] G. Will, K.H. Kossobutzki, J. Less Common Met. 47 (1976) 33.
[17] S. Lee, D.M. Bylander, S.W. Kim, L. Kleinman, Phys. Rev. B 45 (1992) 3248.
[18] Y. Wu, B. Messer, P. Yang, Adv. Mater. 13 (2001) 1487.
[19] L. Cao, Z. Zhang, L. Sun, C. Gao, M. He, Y. Wang, Y. Li, X. Zhang, G. Li, J. Zhang, W. Wang, Adv. Mater. 13 (2001) 1701.
[20] C.J. Otten, O.R. Lourie, M. Yu, J.M. Cowley, M.J. Dyer, R.S. Ruoff, W.E. Buhro, J. Am. Chem. Soc. 124 (2002) 4564.
[21] Y.Q. Wang, X.F. Duan, Appl. Phys. Lett. 82 (2003) 272.
[22] Y. Zhang, H. Ago, M. Yumura, T. Komatsu, S. Ohshima, K. Uchida, S. Iijima, Chem. Commun. 2002 (2002) 2806.
[23] Z. Wang, Y. Shimizu, T. Sasaki, K. Kawaguchi, K. Kimura, N. Koshizaki, Chem. Phys. Lett. 368 (2003) 663.
[24] Q. Yang, J. Sha, J. Xu, Y.J. Ji, X.Y. Ma, J.J. Niu, H.Q. Hua, D.R. Yang, Chem. Phys. Lett. 379 (2003) 87.
[25] T.T. Xu, J.G. Zheng, N. Wu, A.W. Nicholls, J.R. Roth, D.A. Dikin, R.S. Ruoff, Nano Lett. 4 (2004) 963.
[26] W. Hayami, S. Otani, J. Phys. Chem. C 111 (2007) 688.
[27] W. Hayami, S. Otani, J. Phys. Chem. C 111 (2007) 10394.
[28] W. Hayami, S. Otani, J. Phys. Conf. Ser. 176 (2009) 012017.
[29] K. Kirihara, Z. Wang, K. Kawaguchi, Y. Shimizu, T. Sasaki, N. Koshizaki, K. Soga, K. Kimura, Appl. Phys. Lett. 86 (2005) 212101.
[30] K. Kirihara, Z. Wang, K. Kawaguchi, Y. Shimizu, T. Sasaki, N. Koshizaki, H. Hyodo, K. Soga, K. Kimura, J. Vac. Sci. Technol. B 23 (2005) 2510.
[31] K. Kirihara, H. Hyodo, H. Hujihisa, Z. Wang, K. Kawaguchi, Y. Shimizu, T. Sasaki, N. Koshizaki, K. Soga, K. Kimura, J. Solid State Chem. 179 (2006) 2799.
[32] Y. Sato, M. Terauchi, K. Kirihara, T. Sasaki, K. Kawaguchi, N. Koshizaki, K. Kimura, J. Phys. Conf. Ser. 176 (2009) 012029.
[33] D. Li, Y.N. Xu, W.Y. Ching, Phys. Rev. B 45 (1992) 5895.
[34] H. Hyodo, Ph. D. Thesis University of Tokyo (2009).
[35] CPMD, Copyright IBM Corp. 1990-2008, Copyright MPI für Festkörperforschung Stuttgart 1997-2001, (〈www.cpmd.org/〉).
[36] D. Marx, J. Hutter, Modern Methods and Algorithms of Quantum Chemistry, NIC Series Vol. 1, John von Neumann Institute for Computing, Jülich, 2000, pp. 301–449.
[37] W. Andreoni, A. Curioni, Parallel Comput. 26 (2000) 819.
[38] P. Hohenberg, W. Kohn, Phys. Rev. 136 (1964) B864.
[39] W. Kohn, L.J. Sham, Phys. Rev. 140 (1965) A1133.
[40] N. Troullier, J.L. Martins, Phys. Rev. B 43 (1991) 1993.
[41] L. Kleinman, D.M. Bylander, Phys. Rev. Lett. 48 (1982) 1425.

[42] A.D. Becke, Phys. Rev. A 38 (1988) 3098.
[43] C. Lee, W. Yang, R.G. Parr, Phys. Rev. B 37 (1988) 785.
[44] H.J. Monkhorst, J.D. Pack, Phys. Rev. B 13 (1976) 5188.
[45] M.J. van Setten, M.A. Uijttewaal, G.A. de Wijs, R.A. de Groot, J. Am. Chem. Soc. 129 (2007) 2458.
[46] M. Widom, M. Mihalkovic, Phys. Rev. B 77 (2008) 064113.
[47] T. Ogitsu, F. Gygi, J. Reed, Y. Motome, E. Schwegler, G. Galli, J. Am. Chem. Soc. 131 (2009) 1903.
[48] A. Masago, K. Shirai, H. Katayama-Yoshida, Phys. Rev. B 73 (2006) 104102.
[49] S. Lee, D.M. Bylander, L. Kleiman, Phys. Rev. B 42 (1990) 1316.
[50] W. Hayami, S. Otani, J. Phys. Chem. C 112 (2008) 2711.